The investigation of Stefan Luchian heritage paintings – a multi-analytical approach

Andrei Victor Oancea [1], Bogdana Simionescu [2], Laura Elena Ursu [1], Mioara Murariu [1], Marius Dobromir [3], Maria Geba [2,†], Lacramioara Stratulat [2] and Mihaela Olaru [1,*]

[1] "Petru Poni" Institute of Macromolecular Chemistry, 41A Gr. Ghica Voda Alley, 700487 Iasi, Romania"; oancea.victor@icmpp.ro (A.V.O.); ursu.laura@icmpp.ro (L.E.U.); mioara.murariu@icmpp.ro (M.M.); olaruma@icmpp.ro (M.O)

[2] "Moldova" National Museum Complex, 1 Stefan cel Mare si Sfant Square, 700028 Iasi, Romania; simionescubogdana@yahoo.com (B.S.); stratulatlacramioara@yahoo.com (L.S.)

[3] Interdisciplinary Research Institute, Sciences Department, Alexandru Ioan Cuza University of Iasi, 11 Carol I Blvd., 700506, Iasi, Romania; marius.dobromir@uaic.ro (M.D.)

* Correspondence: olaruma@icmpp.ro; Tel.: (+40760289368; M.O.)

The Supporting Information contains data on OM and SEM/EDS microscopy (S1-S5), XPS spectroscopy (S6-S10), original SEM image (S11), original optical image (S12) and discussion of FTIR spectroscopy.

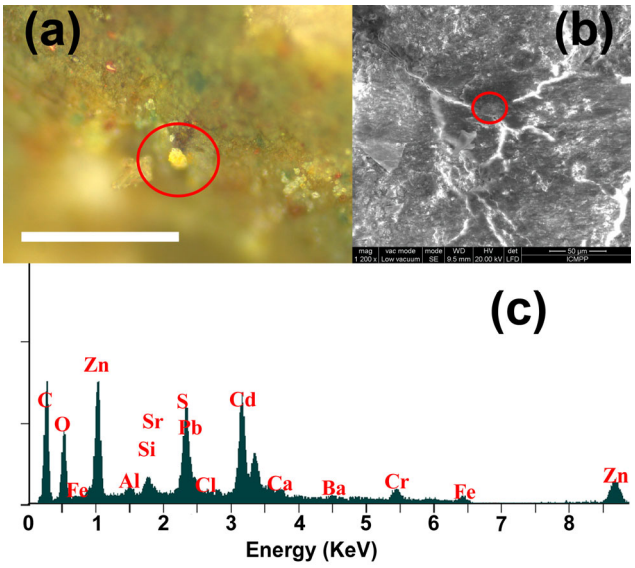


Figure S1. Investigated cadmium yellow grain: (**a**) optical microscopy, scale represent 0.1 mm in length, image was recorded with a 50x objective ; (**b**) SEM image of the investigated area (as identified on the basis of sample morphology and optical microscopy) with the pigment grain highlighted, scale is 50 μm; (**c**) EDS spectrum of the investigated grain revealing high amounts of Cd and S.

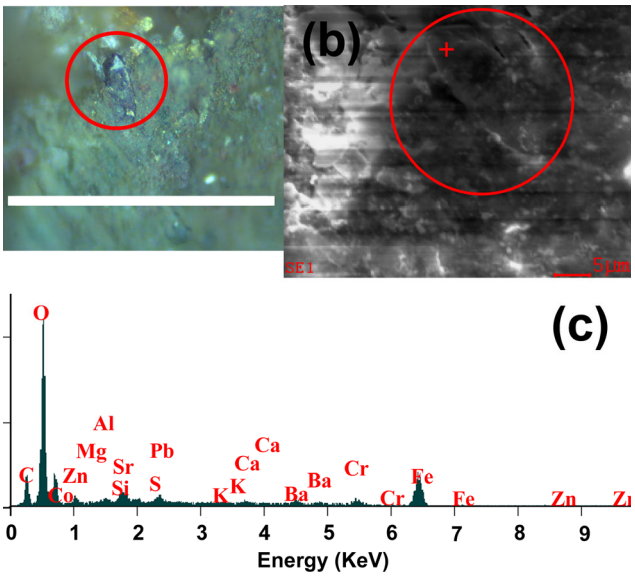


Figure S2. Investigated Prussian blue grain: (**a**) optical microscopy, scale represent 0.1 mm in length, image was recorded with a 100x objective; (**b**) EDS image of the investigated area (as identified on the basis of sample morphology and optical microscopy) with the pigment grain highlighted; scale is 5 μm; (**c**) EDS spectrum of the investigated grain revealing high amounts of Fe.

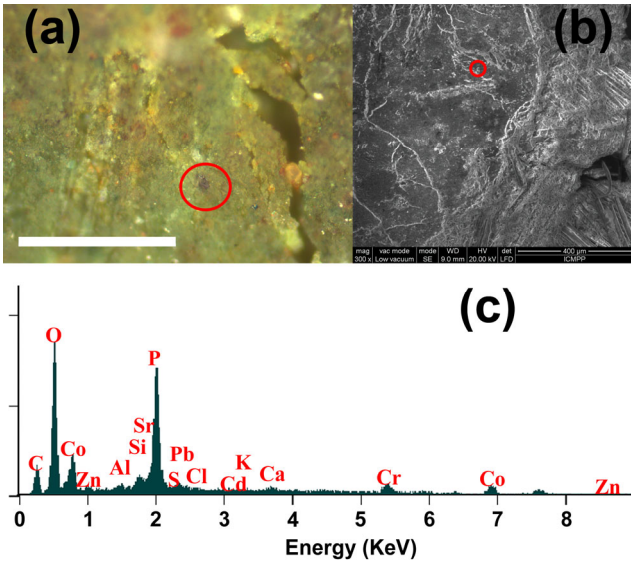


Figure S3. Investigated cobalt purple grain: (**a**) optical microscopy; scale represent 0.1 mm in length, image was recorded with a 50x objective (**b**) SEM image of the investigated area (as identified on the basis of sample morphology and optical microscopy) with the pigment grain highlighted, scale is 500 μm; (**c**) EDS spectrum of the investigated grain showing significant amounts of Co and P.

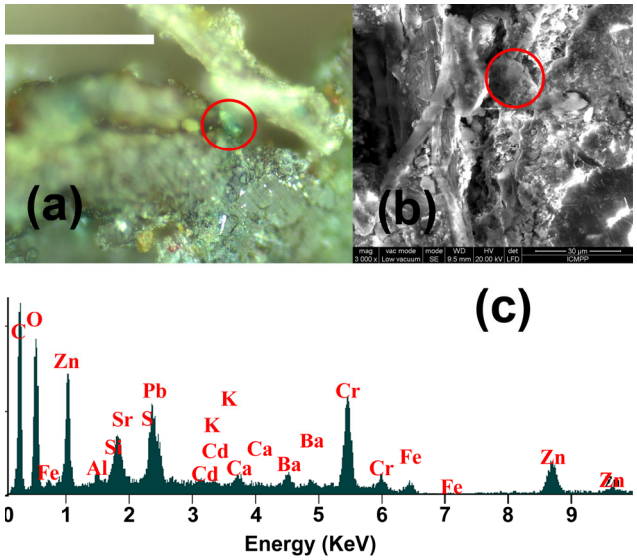


Figure S4. Investigated chrome green grain: (**a**) optical microscopy, scale represent 0.1 mm in length, image was recorded with a 50x objective; (**b**) SEM image of the investigated area (as identified on the basis of sample morphology and optical microscopy) with the pigment grain highlighted, scale is 30 μm; (**c**) EDS spectrum of the investigated grain exhibiting high amounts of Cr.

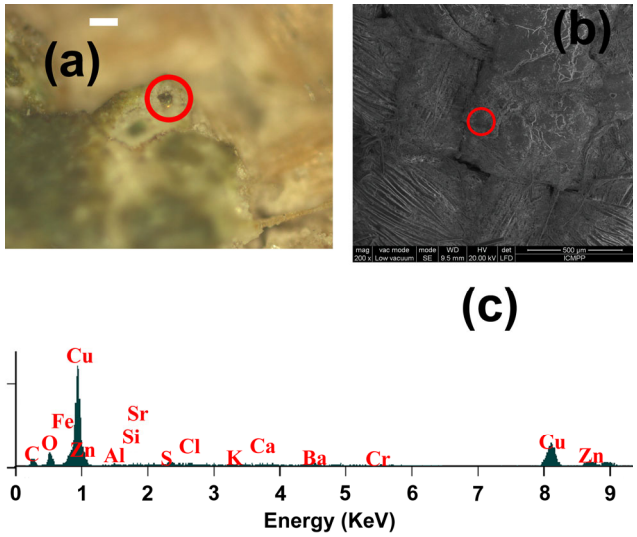


Figure S5. Investigated green copper grain: (**a**) optical microscopy, scale represent 0.1 mm in length, image was recorded with a 10x objective; (**b**) SEM image of the investigated area (as identified on the basis of sample morphology and optical microscopy) with the pigment grain highlighted, scale is 500 μm; (**c**) EDS spectrum of the investigated grain showing high amounts of Cu.

Supplementary Table S1. The EDS investigations în which the atomic concentration of various grains (the grains that were also observed under optical microscopy, beside the pigment assignment) is mentioned

Pigment	C	N	O	Co	Al	Si	Sr	S	Pb	K	Ca	Ba	Cr	Fe	Zn	Hg	Mn	In	Cl	Sn	Mg	P	Cd	Na	Ni	Cu	F
Barium white + significant Co and Zn	52.81		32.08	1.14	0.36	0.35	0.51	5.4	0.24	0.02	0.11	5.26	0.62	0.2	0.74												
Barium white + significant Co and Zn	58.02		30.99	0.75	0.18	0.33	0.24	3.39		0.1	0.72	3.69	0.34	0.22	0.61		0.2			0.11	0.11						
Barium white	23.31		48.28		0.25	0.72	1.22	11.13	0.54		0.19	12.83	0.67		0.86												
CaCO3 + Zinc White	58.44	0.59	19.48		0.54	0.74	0.34	1.28	0.18	0.14	8.89	1.16	0.82	0.31	6.67	0.42											
Zinc White	65.6		24.08			0.31		1.49			0.35	1.68			6.07				0.38	0.05							
Zinc white + Barium white + significant Co	64			0.75	0.15	0.28	0.22	1.95	0.15		0.37	2.5	0.27		5.29												
gypsum	64.45		22.55		0.4	1.05	0.18	4.7	0.34		5.23	0.15	0.35	0.15	0.36						0.1						
Lead white	58.36		27.97		0.43	0.66	1.02	1.72	6.82		0.27	0.29	1.22	0.31	0.94												
Lead white	47.07		33.14		1.82	1.84	1.34	1.77	7.85		0.35	0.42	2.18	0.86	1.37												
Strontium yellow	50.35		39.41		0.62	0.79	2.3	0.25	0.32		0.21		3.17	1.26	0.86	0.34						0.12					
Hematite + viridian	41.82		23.33		1.05	1.73	0.73	0.41	0.6	0.26	0.42	0.29	12.1	15.31	0.74				0.15				0.24		0.81		
Cadmium yellow	47.03		21.27		0.28	0.53		13.23					1.66		1.83	0.52							13.64				
Cadmium yellow	56.16		18.78		0.31	0.4	0.4	9.48	0.43	0.09	0.4	0.23	1.15	0.36	1.15	0.33			0.18				10.17				
Cadmium yellow / OM	67.25		20.33		0.34	0.57	0.23	2.62	0.36		0.34	0.21	0.7	0.38	3.43				0.12				3.11				
Prussian blue / OM + significant Co	35.58		52.76	2.74	0.38	0.63	0.21	0.27	0.1	0.02	0.23	0.39	0.72	5.33							0.22						
Hematite	35.69	3.54	44.37		0.66	0.84	0.59	0.37	0.64	0.13	0.28	0.15	1.52	10.07	0.8		0.23		0.13								
Cobalt purple / OM	38.53		49.59	1.28	0.28	0.51	0.38	0.16	0.13	0.06	0.25		0.92		0.4							7.51					
Vermillion	50.74		22.31		0.42	0.93		11.63					1.55			12.43											
Vermillion	52.88		27.64		0.4	1.31	0.37	6.4	0.15		0.78	0.2	1.33	0.44		6.44											
Viridian / OM	67.15		21.15		0.34	0.15		0.61	0.85	0.1	0.33	0.44	4.03	0.47	3.49	0.11							0.11				
Viridian	59.26		27.65		0.56	0.84	0.48	0.3	0.27		0.52	0.23	8.02	0.44							0.13						
Viridian	26.76		51.61		0.47	0.55	0.46	0.4	0.16	0.21	0.38	0.26	13.72	2.8	0.76				1.3							0.16	
Viridian	44.91		43.57		0.24	0.33	0.31	0.16	0.21		0.17		9.06		0.9						0.14						
burnt umber / Sienna	37.36		46		0.57	0.77	0.46	0.26	0.14	0.22	0.45	1.02	1.16	0.19	0.78		10.5		0.08				0.03				
Indium yellow	35.81		25.56		1.86	2.15	1.24	1.37			0.76	0.40	1.22		0.98			22.42			1.41			2.78			2.05

Indium yellow	36.21	33.69	1.36	1.89	0.81		0.34		0.33	0.07	1.46	0.33	1.03	20.29		2.19	
Copper pigment / OM	47.27	17.46	1.46	0.47	0.3	0.87		0.56	0.64	1.04	0.74		6.09		0.67		21.06

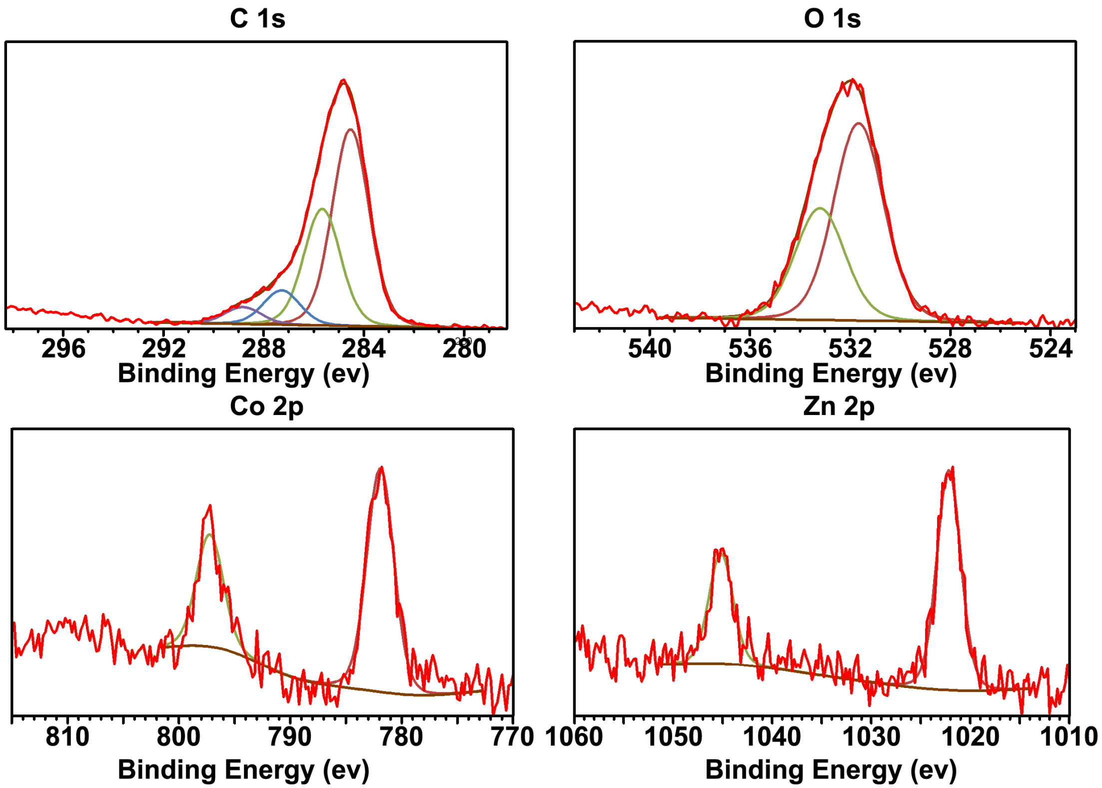


Figure S6. XPS spectra of relevant elements – sample from "Chrysanthemums" painting, sample LIIA – canvas fragment with black smudges. Spectrum was recorded from pigment area - blackish smudges (LIIA analysis point 1 in XPS table): (**a**) C 1s spectrum and peak fitting, (**b**) Co 2p spectrum and peak fitting, (**c**) O 1s spectrum and peak fitting, (**d**) Zn 2p spectrum and peak fitting.

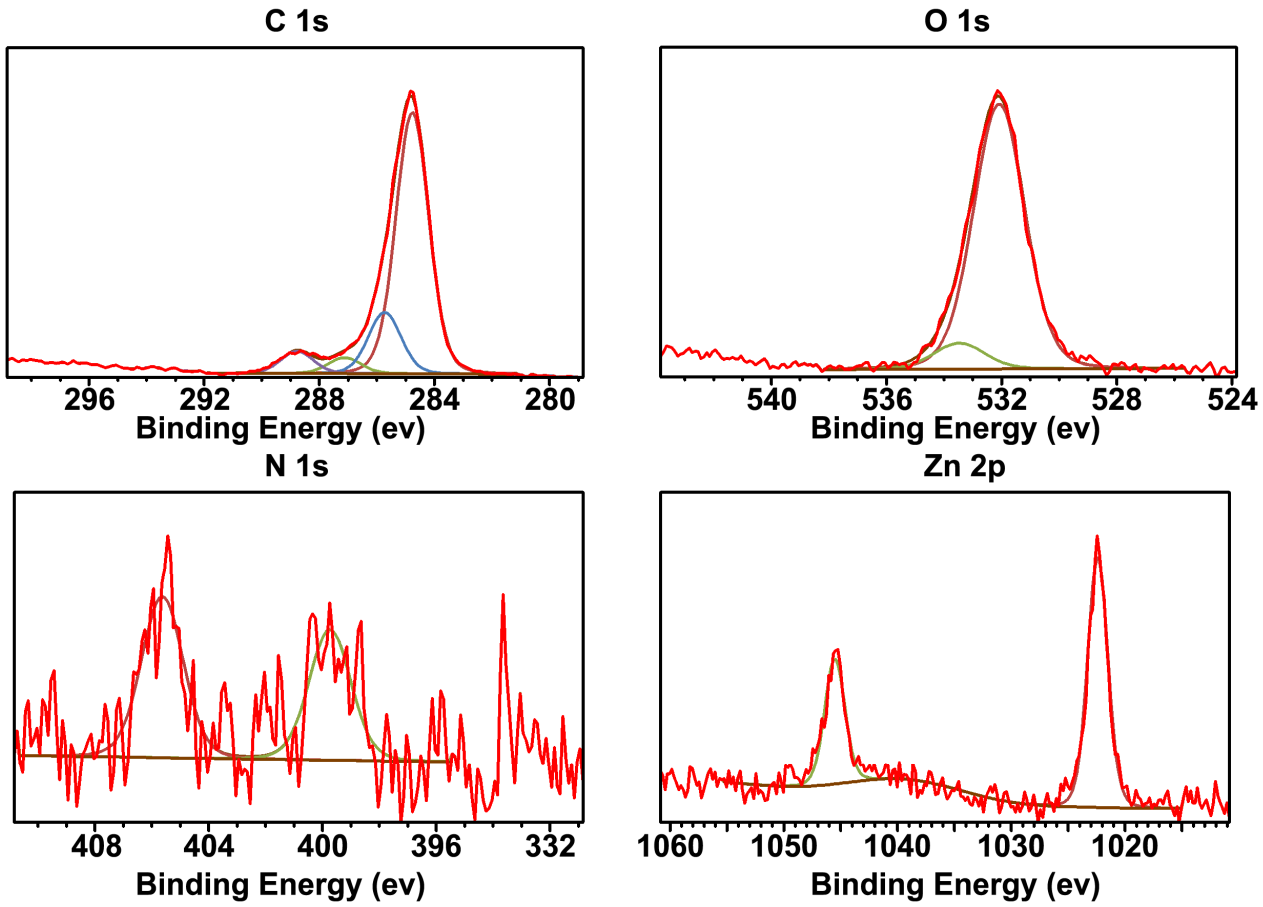


Figure S7. XPS spectra of relevant elements – sample from "Chrysanthemums" painting, sample LIIA – canvas fragment with black smudges. Spectrum was recorded from canvas area area (LIIA canvas in XPS table): (**a**) C 1s spectrum and peak fitting, (**b**) N 1s spectrum and peak fitting, (**c**) O 1s spectrum and peak fitting, (**d**) Zn 2p spectrum and peak fitting.

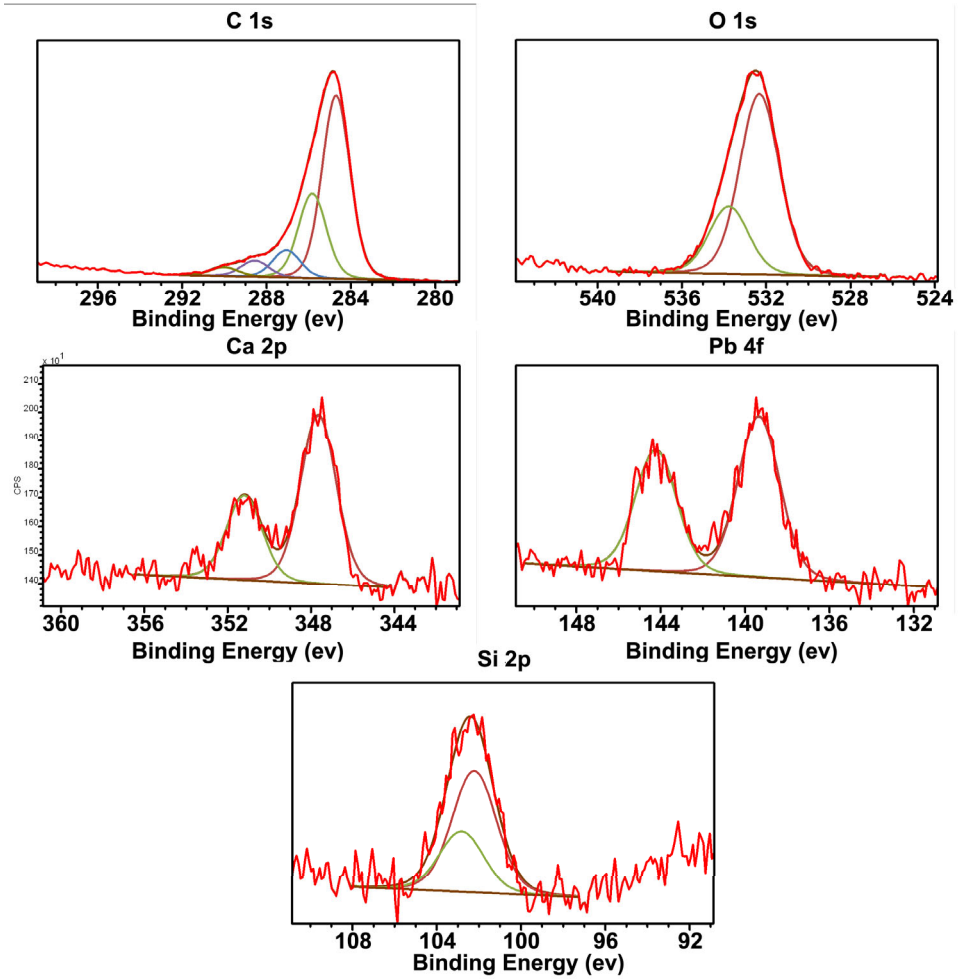


Figure S8. XPS spectra of relevant elements – sample from "Roses" painting, sample LIB – small grains (LIIB in XPS table): (**a**) C 1s spectrum and peak fitting, (**b**) O 1s spectrum and peak fitting, (**c**) Ca 2p spectrum and peak fitting, (**d**) Si 2p spectrum and peak fitting, (**e**) Pb 4f spectrum and peak fitting.

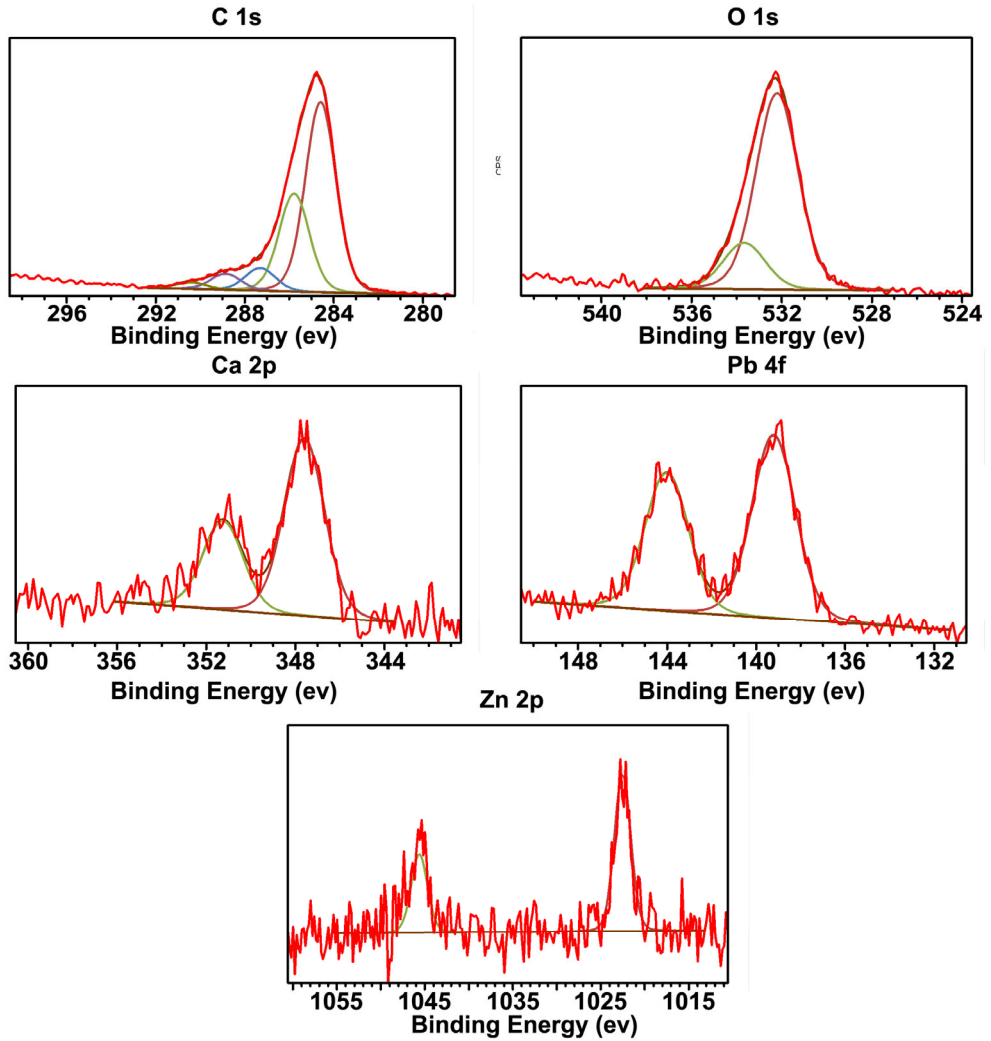


Figure S9. XPS spectra of relevant elements – sample from "Chrysanthemums" painting, sample LIIB – small grains (LIIB in xps table): (a) C 1s spectrum and peak fitting, (b) O 1s spectrum and peak fitting, (c) Zn 2p spectrum and peak fitting, (d) Ca 2p spectrum and peak fitting, (**e**) Pb 4f spectrum and peak fitting.

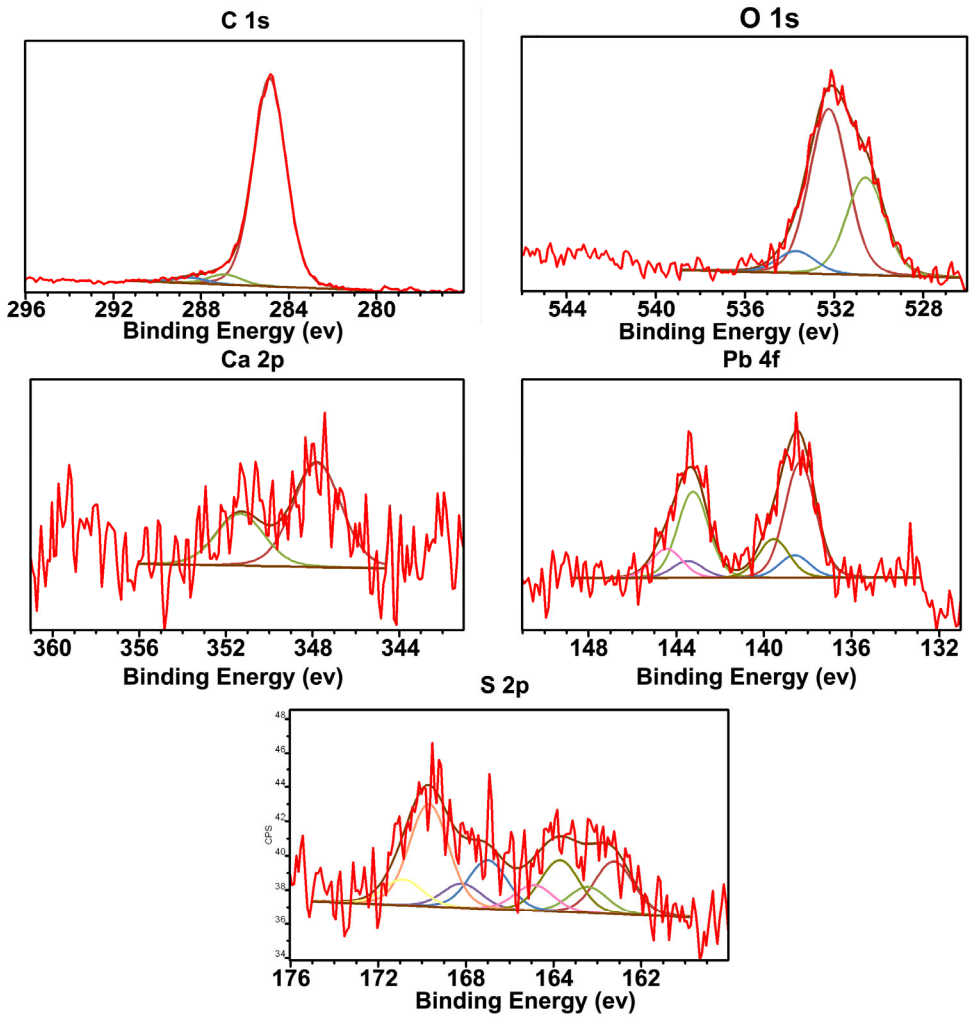


Figure S10. XPS spectra of relevant elements – sample from "Chrysanthemums" painting, sample LIIA – canvas fragment with black smudges. Spectrum was recorded from pigment area - blackish smudges (LIIA analysis point 2 in XPS table): (**a**) C 1s spectrum and peak fitting, (**b**) O 1s spectrum and peak fitting, (**c**) Ca 2p spectrum and peak fitting, (**d**) Ba 3d spectrum and peak fitting, (**e**) Pb 4f spectrum and peak fitting, (**f**) S 2p spectrum and peak fitting, (**g**) Zn 2p spectrum and peak fitting.

Supplementary Table S2. The assignments of the XPS bands of LIB, LIB_V, LIIA analysis point 1, LIIA analysis point 2, LIIA canvas, LIIA indium oxide grain spectra

XPS						Element bands	Tentative band assign-ment	Material
LIB	LIB_v	LIIA analysis point 1	LIIA analysis point 2	LIIA can-vas	LIIA indium oxide grain			
284.71	284.59	284.53		284.77		C 1s	C-C/C-H	Linseed oil [1]
285.83	285.78	285.66		285.13			C-O/C-OH/C-O-C	
287.06	287.3	287.28		287.12			C=O	
288.56	288.85	288.82		288.77			O-C=O	
290							$CaCO_3$	Calcium carbonate [2]
	290.4						$PbCO_3$	cerrusite [3]
			284.87		284.83		C-C/C-H	adventitious carbon [4]
			286.92		286.61		C-O-C	
			288.48		288.91		O-C=O	
					530	O 1s	In_2O_3	Indium yellow [5]
			530.38				PbO	Lead(II) oxide [6]
532.32	532.2	531.66	532.24	532.08	531.89		C-O-C/O-C=O/C=O/ Co doped ZnO /ZnO/SiO_2/$Pb(OH)_2$	linseed oil [1]/adventitious carbon [4]/Co doped ZnO [7,8]/zinc white [9]/quartz [5]/lead hydroxyde [5]

533.77	533.66	533.2	533.7	533.47	533.15		O-C=O/$CaCO_3$/$PbCO_3$	linseed oil [1]/adventitious carbon [4]/calcium carbonate [2]/lead carbonate [10]
		1022.18				Zn $2p_{3/2}$	Co doped ZnO	Co doped ZnO [7,8]
		1045.2				Zn $2p_{1/2}$	Co doped ZnO	
	1022.52		1022.44	1022.4		Zn $2p_{3/2}$	ZnO	Zinc white [9]
	1045.63		1045.25	1045.52		Zn $2p_{1/2}$	ZnO	
		781.92				Co $2p_{3/2}$	Co doped ZnO	Co doped ZnO [7,8]
		797.23				Co $2p_{1/2}$	Co doped ZnO	
				399.74		N 1s	Amide linkage	Protein [11]
				405.63		N 1s	adsorbed NO_3	Nitric oxydes adsorbed on the surface of the samples [12]
347.64	347.64		347.79			Ca $2p_{3/2}$	$CaCO_3$ / $CaSO_4$	Calcium carbonate [2]/gypsum [13]
351.19	351.19		351.34			Ca $2p_{1/2}$	$CaCO_3$	
			790.62			Ba $3d_{5/2}$	$BaSO_4$	Barium white [2]
			795.95			Ba $3d_{3/2}$	$BaSO_4$	
139.35	139.19					Pb $4f_{7/2}$	$PbCO_3$	Cerrusite [3]
144.23	144.07					Pb $4f_{5/2}$	$PbCO_3$	
			138.85			Pb $4f_{7/2}$	PbO	Lead (II) oxide [6]
			143.23			Pb $4f_{5/2}$	PbO	
			138.6			Pb $4f_{7/2}$	PbS/$Pb(OH)_2$	Galena [5]/ lead hydroxide [5]
			143.48			Pb $4f_{5/2}$	PbS/$Pb(OH)_2$	
			139.55			Pb $4f_{7/2}$	$PbSO_4$	Lead sulfate [5]
			144.43			Pb $4f_{5/2}$	$PbSO_4$	
			161.25			S $2p_{3/2}$	PbS	Galena [5]
			162.43			S $2p_{1/2}$	PbS	

	163.71		S $2p_{3/2}$	Elemental S	Elemental S [14]
	164.89		S $2p_{1/2}$	Elemental S	
	167		S $2p_{3/2}$	Adsorbed SO_2	Adsorbed SO_2 [15]
	168.18		S $2p_{1/2}$	Adsorbed SO_2	
	169.69		S $2p_{3/2}$	$PbSO_4$/$CaSO_4$/$BaSO_4$	Lead sulfate [2] /gypsum [2]/ barium white [2]
	170.87		S $2p_{1/2}$		
		443.39	In $3d_{5/2}$	indium metal	Indium metal [16]
		450.85	In $3d_{3/2}$	indium metal	
		444.36	In $3d_{5/2}$	In_2O_3	Indium yellow [16]
		451.87	In $3d_{3/2}$	In_2O_3	
102.24			Si $2p_{3/2}$	quartz	Impurity in red or yellow ochres [5]
102.84			Si $2p_{1/2}$	quartz	

In the case of lines 11 and 12, where the assignment of the O 1s bands is performed, the oxygen assigned to that characteristic value is highlighted in red

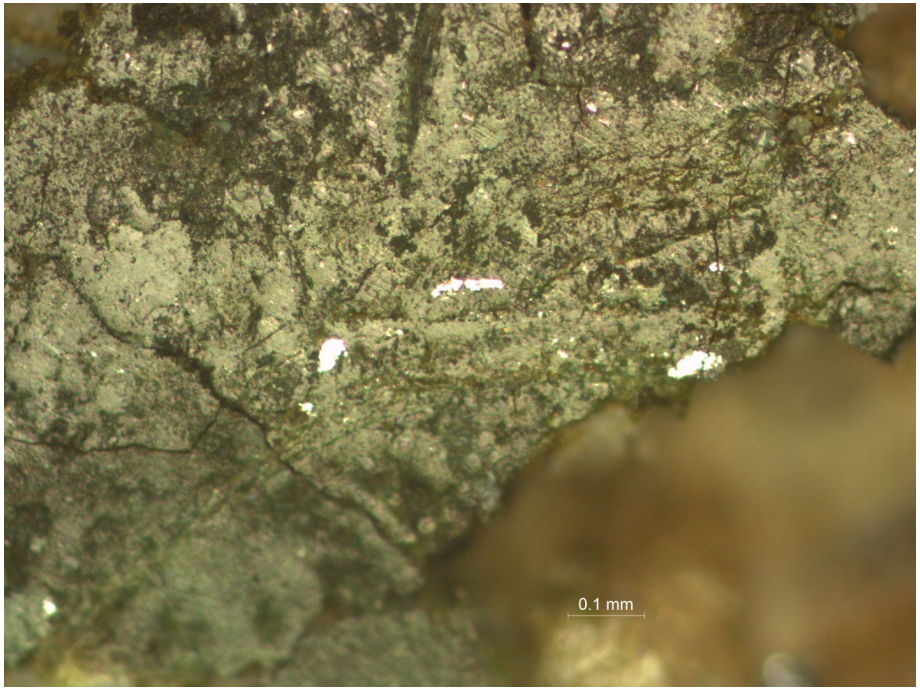


Figure S11. The original OM image used in Figure 1a in manuscript.

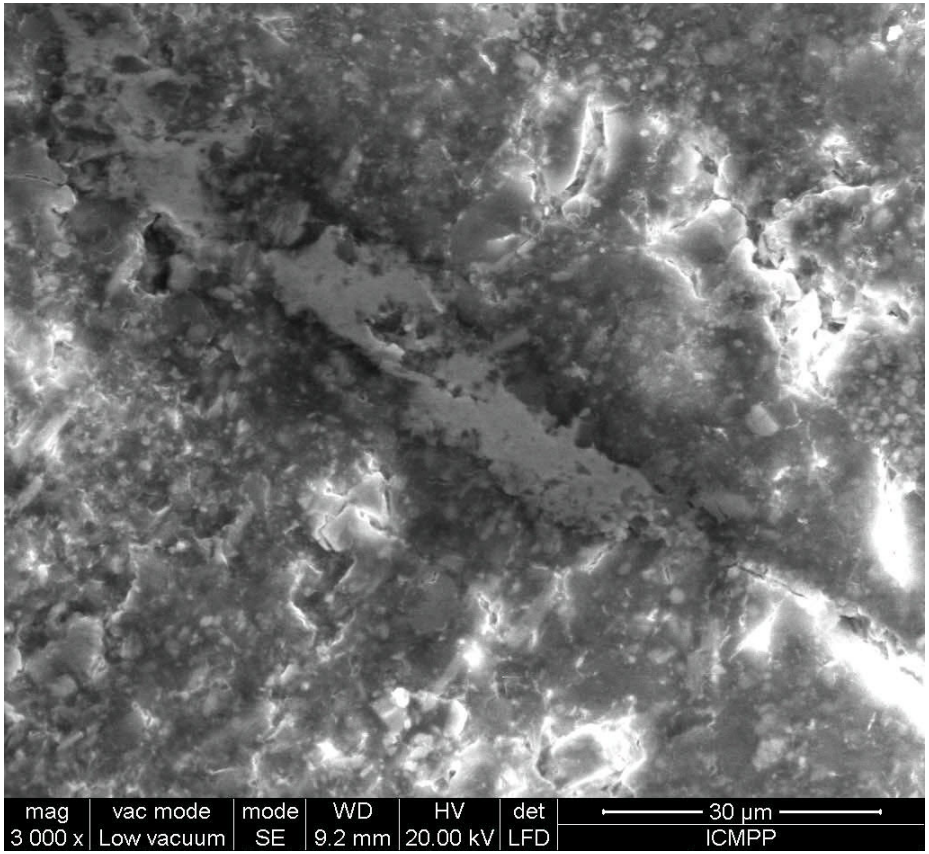


Figure S12. The original SEM image used in Figure 1b in manuscript.

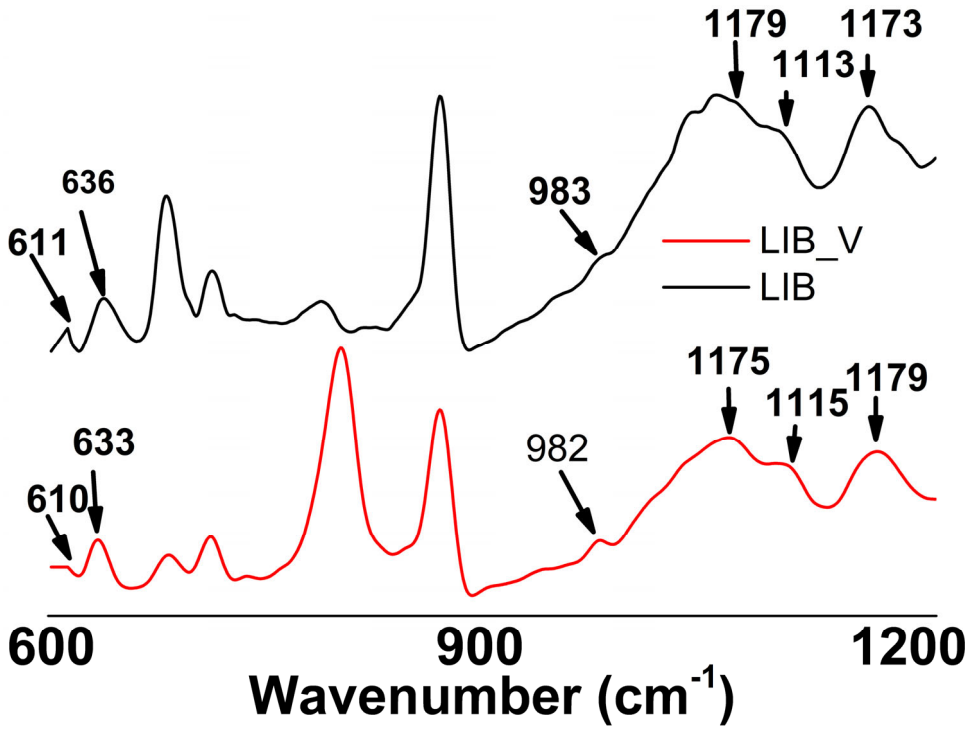


Figure S13. 600-1200 cm^{-1} region of FTIR spectra for LIB and LIB_V, with the position of the characteristic bands of barium white ($BaSO_4$) marked by arrows

Supplementary Table S3. The assignments of the absorption bands (portable Raman) of Roses and Chrysanthemums paintings

Portable Raman		Pigment	Tentative band assignment
Roses	Chrysanthemums		
	1049	Lead white [17]	ν_1 CO_3^{2-} symmetric stretching
	1372		ν_3 CO_3^{2-}antisymmetric stretching
	(pts. 8, 11, 12, 18)		
453		Barium white [18]	ν_1 symmetric bending of SO_4^{2-}
462			ν_2 bending of SO_4^{2-}
989			ν_1 symmetric stretching of SO_4^{2-}
(pts. 3, 7, 8, 11, 13)			
386		Zinc white [19]	A1(TO) mode
435			E2 mode
(pt. 6)			
	863	Strontium yellow [20]	ν_1 symmetric of CrO_4
	892		ν_3 antisymmetric stretching modes of CrO_4
	(pts. 13, 14)		
253		Vermillion [21]	A_1 stretching mode of HgS
283			Eu stretching mode of HgS
343			Eu stretching mode of HgS
(pts. 1, 4, 5, 6, 12, 15)			
1291	1291	alizarin crimson (PR83)	CO stretching, CC stretching, CCC in-
	(pt. 9)	[22]	plane bending
1327	1327		CC stretching
1482	1482		CO stretching, CC stretching, CH in-
(pt. 14)			plane bending
	1298	Beeswax [23]	$\delta(CH_2, CH_3)$ deformations
	1442		$\delta(CH_2$ deformations)
	(pt. 8)		

Supplementary Table S4. The assignments of the absorption bands (μ-Raman) of LIB, LIB_V, LIIA, LIIB, LIIB_V, LIIA_pz1 and LIIA_pz2 samples

μ-Raman							Pigment	Tentative band assignment
LIB	LIB_V	LIIA	LIIB	LIIB_V	LIIA_pz1	LIIA_pz2		
		544					Ultramarine [24]	ν_1 symmetric stretching vibration of S^{3-} ion
		140					Massicot [25]	combination band
		292						B_{2g} and B_{3g}
		226					Hematite [26]	A_{1g} mode, symmetric bends of Fe-O
		245						Eg mode, symmetric stretch of Fe-O
		292						Eg mode, symmetric stretch of Fe-O
		408						Eg mode, symmetric stretch of Fe-O
		609						Eg mode, symmetric stretch of Fe-O
		655						Eu mode, IR active LO
		196					Cobalt phosphate [27]	external mode of cobalt phosphate
		1365					Carbon black [28]	D1 band due to the occurrence of disordered structures
		1585						G band coming from the sp^2 carbon planar configuration of graphite
		145					Anatase (likely component of red ochre) [29]	B_{1g} band
453							Barium white [18]	ν_1 symmetric bending of SO_4^{2-}
462								ν_2 bending of SO_4^{2-}
989								ν_1 symmetric stretching of SO_4^{2-}
253	253						Vermillion [21]	A_1 stretching mode of HgS
283	283							Eu stretching mode of HgS
343	343							Eu stretching mode of HgS

Supplementary Table S5. The assignments of the absorption bands (FTIR) of LIB, LIB_V, LIIA, LIIB, LIIB_V, LIIA_pz1 and LIIA_pz2 samples

LIB	LIB_v	LIIA	LIIB	LIIB_V	LIIA_pz1	LIIA_pz2	Oil/Pigment	Tentative band assignment
611	611	610	618	611	611	611	Goethite [30], gypsum [31], barium white [32], zinc oxalates [33], animal glue [34-36]	FeO_6 lattice, out-of-plane bending of SO_4^{2-}, asymmetric bending of SO_4^{2-}, water libration, out-of-plane bending of N–H or C–H vibrations
637	633	634	643	638	638	643	Cobalt phosphate [37], viridian [38], barium white [32], ultramarine [39], $PbSO_4$ [31]	bending of O-P-O group, Cr-O stretching, asymmetric bending vibrations of SO_4^{2-}, symmetric stretching of (Si, Al)-O-Si), out-of-plane bending of SO_4^{2-}
		662	662	667	666	667	Goethite [30], cadmium yellow [40]	combination band, Cd-S stretching, OCO bending
680	682	685		676	678	677	Lead white [41], hydrocerussite [41], gypsum [31], cobalt phosphate [37]	in-plane bending vibration of CO_3^{2-}, asymmetric bending of SO_4^{2-}, Co-O lattice vibration mode
,		698	699		703	699	Hydrocerussite [41], quartz [42], ultramarine [39]	in-plane bending modes of CO_3^{2-}, Si-O symmetrical bending, symmetric stretching of (Si, Al)-O-Si)
712	712			713	715	715	Calcite [42], ultramarine [39]	planar bending of CO_3^{2-}, symmetric stretching of (Si, Al)-O-Si)
723		725	722		723	719	Viridian [38], cadmium yellow [40], beeswax [48]	Cr-O stretching, Cd-S stretching, $\delta(CH_2)_n$ non-planar skeletal deformation
747	740	750					Cobalt-doped zinc oxide [43], zinc oxalates [33]	microstructural changes, water libration
		776					Quartz [13], kaolinite [15]	Si-O symmetrical stretching, symmetric stretching of Si–O–Si inter tetrahedral bonds
794	803	793	808		804	801	Quartz [42], goethite [30], kaolinite [44]	Si-O symmetrical stretching, out-of-plane OH deformational mode, symmetric stretching of Si–O–Si inter tetrahedral bonds
849		842	852		852	852	Lead white [41], strontium yellow [45], animal glue [34-36]	out-of-plane bending vibration of CO_3^{2-}, Cr-O symmetric stretching, skeletal vibrations of C–C and C–N bonds

872	872	876	875	875	879	877	Strontium yellow [45], gypsum [31], calcite [42]	Cr-O asymmetric stretching mode, OH bending, out-of-plane bending of CO_3^{2-}
		886					Strontium yellow [45]	Cr-O asymmetric stretching mode
		905	897	900	905	899	Strontium yellow [45], goethite [30]	Cr-O asymmetric stretching mode, in plane OH deformational mode
927		930			931		Hydrocerussite [41], strontium yellow [45], kaolinite [44], shellac [46,47], animal glue [34-36]	δ Pb-OH, Cr-O asymmetric stretching mode, OH deformation, associated to $2Al^{3-}$, OH out-of-plane bending, C-C stretching, skeletal vibrations of C–C and C–N bonds
953	945		956				Beeswax [48], shellac [46,47], cobalt phosphate [37], $PbSO_4$ [31]	bending of C–H units, CH out-of-plane bending, bending of O-P-O group, asymmetric stretching of SO_4^{2-}
985	984		986	986	985	985	Aged linseed oil [49], cobalt phosphate [37], barium white [32], animal glue [34-36]	CH wagging of isolated trans CH=CH groups, P-O stretching, symmetric stretching of SO_4^{2-}, skeletal vibrations of C–C and C–N bonds
	1004	1008	1004	1003	1004	1003	Kaolinite [44], gypsum [31], ultramarine [39]	Si-O-Al stretching, symmetric stretching of SO_4^{2-}, asymmetric stretching of (Si, Al)-O-Si)
1028	1023	1030	1028	1030	1028	1027	Kaolinite [44], cobalt phosphate [37], animal glue [34-36]	Si-O-Si stretching, antisymmetric stretching of PO_4^{3-} units, C-C stretching, C–O stretching
1045	1045		1054	1055	1054	1053	Lead white [41], hydrocerussite [41], shellac [46,47], cobalt phosphate [37], $PbSO_4$ [31]	symmetric stretching of CO_3^{2-}), CO stretching, CH bending, antisymmetric stretching of PO_4^{3-} units, asymmetric stretching of SO_4^{2-}
1067		1064					Cobalt phosphate [37]	antisymmetric stretching of PO_4^{3-} units
1079	1075	1087					Barium white [32], quartz [42], cobalt-doped zinc oxide [43], animal glue [34-36]	asymmetric stretching of SO_4^{2-}, Si-O stretching, stretching vibration of H_2O in a Cu-Zn-O lattice, vibration coupling of specific amino acid side chains or peptide groups

			1104	1105	1104	1103	Aged linseed oil [49], ultramarine [39], animal glue [34-36]	CO stretching in C-O-C groups from esters, Si-O stretching, δ (CH)
1115	1115						Shellac [46,47], barium white [32]	CH bending, asymmetric stretching of SO_4^{2-}
		1165	1159	1162	1156	1156	Aged linseed oil [49], quartz [42], gypsum [31], shellac [46,47]	CO stretching in C-O-C groups from esters, Si-O asymmetrical stretching, symmetric bending of SO_4^{2-}, COO stretching, CH bending
1173	1179						Beeswax [48], barium white [32], $PbSO_4$ [31]	C-O-C stretching of ester groups, asymmetric stretching of SO_4^{2-}
			1201	1208	1200	1202	Aged linseed oil [49], animal glue [34-36]	CO stretching from alcohols, C–N stretching vibrations
				1241	1237	1236	Aged linseed oil [49], shellac [46,47], animal glue [34-36]	CH_2 twisting of esters, COO stretching, CC stretching, CH bending, amide III (C–N stretching, N–H deformation)
1251	1249	1251	1250		1257	1260	Aged linseed oil [49]	CO stretching in C-O-C groups from esters
1285		1286	1278	1284	1281	1280	Viridian [38]	Symmetric stretching of CO_2ó chemisorbed species
1317	1313	1319	1317	1316	1315	1315	Copper oxalates [33], zinc oxalates [33]	symmetric C=O stretching
			1336	1336	1339	1338	Animal glue [34-36]	CH_2 deformation
1359	1362	1357					Copper oxalates [33], zinc oxalates [33]	symmetric C=O stretching
			1371	1373	1371	1370	Aged linseed oil [49], shellac [46,47]	CH bending, CH_3 bending
1398	1396	1400		1394	1396	1396	Lead white [41]	antisymmetric stretching of CO_3^{2-}
		1414	1412	1406	1413	1412	Aged linseed oil [49], shellac [46,47], lead oleates [50], lead palmitates [50], animal glue [34-36]	CO bending of acid groups, CH bending of $–CH_2$-COO groups, OH bending, symmetric stretching of COO^- ions
1421	1425	1432	1423	1423	1426	1426	Copper oleates [51], calcium palmitates [51], manganese palmitates [50]	Symmetric stretching vibrations of carboxylate units, asymmetric stretching of $CO_3^{2–}$

1456	1452	1454	1458	1455	1452	1455	Aged linseed oil [49], calcium palmitates [51], shellac [46,47], zinc oleates [48], animal glue [34-36], beeswax [48]	CH_3 asymmetric bending and CH_2 scissoring, CH_2 bending, CO stretching, OH deformation of primary/secondary alcohol, bending of CH_2, CH_2 scissoring, CH planar deformation
			1465	1464	1464	1464	Lead palmitates [50], zinc oleates [48], copper oleates [51], manganese palmitates [48]	CH_2 bending
		1488	1473	1473	1470	1470	Lead oleates [52]	asymmetric stretching vibrations of carboxylate groups
				1492	1487	1485	Lead oleates [50]	asymmetric stretching of COO- ions
				1507	1507	1506	Lead oleates [50]	asymmetric stretching of COO- ions
			1514	1515	1516	1515	Lead palmitates [50]	asymmetric stretching of COO^- ions
			1532	1527			Zinc oleates [48], animal glue [34-36]	asymmetric stretching of COO^- ions, amide II (CN stretching, NH bending)
1538	1534	1540	1538	1544	1538	1538	Zinc oleates [48], lead palmitates [50], zinc oleates [48]	asymmetric stretching of acetate ions, asymmetric stretching of COO^- ions
		1553	1548	1557	1554	1554	Zinc oleates [48]	asymmetric stretching vibrations of carboxylate groups
				1564			Manganese palmitate [48]	asymmetric stretching vibrations of carboxylate groups
1570		1574			1576	1576	Calcium palmitates [51]	asymmetric stretching vibrations of carboxylate groups
1593	1592	1593	1597	1593			Copper oleates [51], cobalt phosphate [34]	asymmetric stretching vibrations of carboxylate groups, H-OH bending
		1611			1612	1613	Aged linseed oil [49]	C=O stretching of carboxylic acids, aldehydes and α/β unsaturated ketones
1626	1622		1627	1625			Viridian [38], barium white [32], animal glue [34-36]	hydration water, symmetric stretching of SO_4^{2-}, amide I (C=O stretching)
		1633		1635	1630	1635	Goethite [30], zinc oxalates [33]	OH bending mode, asymmetric C=O stretching, HOH bending
1647	1643	1646	1653	1654	1648	1647	Aged linseed oil [49], goethite [30], shellac [46,47]	C=C stretching, C=O stretching of aldehyde or acid compounds, OH bending mode, C=C stretching deriving

								from jalaric and shellolic acids, CO stretching
	1673	1666		1671	1671	1670	Copper oxalates [33]	asymmetric C=O stretching, HOH bending
		1697			1695	1692	Goethite [30], cobalt-doped zinc oxide [43]	OH bending mode, H-OH bending
1712	1714	1714	1714		1714	1714	Aged linseed oil [49], beeswax [48], shellac [46,47]	C=O stretching of free carboxylic acids and saturated ketones, CO stretching of carboxylic groups, C=O stretching
1735	1735	1736	1730	1735	1730	1730	Lead white [41], aged linseed oil [49], beeswax [48], shellac [46,47]	$\nu_1 + \nu_4$ combination modes of CO_3^{2-}, ester C=O stretching of triglyceride constituents, C=O stretching of ester groups
					1766	1768	Aged linseed oil [49]	C=O stretching of γ-lactones
1795	1797	1786			1790	1789	Calcite [42]	stretching of CO_3^{2-}
2092	2094	2091	2091	2086	2087	2091	Gypsum [31]	combination of 1st overtone and asymmetric stretching of SO_4^{2-}
2358		2355	2356		2355	2356	Viridian [38], cobalt-doped zinc oxide [43]	CO_2 adsorption
	2729	2736			2740	2733	Aged linseed oil [49]	overtone CH in-plane deformation of aliphatic aldehydes
2850	2853	2851	2852	2853	2850	2850	Aged linseed oil [49], beeswax [48], shellac [46,47], animal glue [34-36]	symmetric CH stretching of CH-CH_2 and CH_3 groups, asymmetric CH stretching of CH_3, CH_2 and CH groups, CH_2 stretching
2918	2921	2918	2921	2922	2920	2920	Aged linseed oil [49], beeswax [48], shellac [46,47], barium white [32], animal glue [34-36]	asymmetric CH stretching of alkyl CH-CH_2 and CH_2 groups, asymmetric stretching of CH_2 group, CH_3 stretching, symmetric OH stretching
		2956			2962	2962	Beeswax [48], unsaturated fatty acids [53]	asymmetric stretching of CH_3 group, $CH(CH_3)$ asymmetric stretching
					3008		Zinc soap of unsaturated fatty acids [54]	CH=CH stretching
					3035		Zinc soap of unsaturated fatty acids [54]	CH=CH trans stretching

3085		3079					Cobalt phosphate [34]	OH stretching
			3103	3107				
		3143					Goethite [30]	OH stretching
					3190	3190		
			3241					
			3279	3270			Animal glue [34-36]	NH stretching, hydrogen bonding
			3283	3290				
		3319		3313		3306	Beeswax [48]	
				3321				
				3339	3333		Aged linseed oil [49]	OH stretching (hydroperoxides, alcohols)
3350	3344		3350		3359	3355	Beeswax [48]	stretching vibrations of hydroxyl groups
3388	3393	3393	3394	3391	3390	3385	Goethite [30], gypsum [31], shellac [46,47], cobalt-doped zinc oxide [43], zinc oxalates [33]	ν H-OH, OH stretching, OH stretching vibrations of carboxylic and hydroxylic groups, stretching vibration of H_2O in a Cu-Zn-O lattice
			3423				Viridian [38], barium white [32]	OH stretching, anti-symmetric OH stretching
3460	3455							
3528							Hydrocerussite [41]	stretching mode of OH group
			3542					
			3609	3602				
	3622						Kaolinite [44]	inner hydroxyl ions
	3662						Kaolinite [44]	outer hydroxyl ions
	3727						Kaolinite [44]	outer hydroxyl ions

As regards viridian ($Cr_2O_3 \cdot 2H_2O$), the broad band located at around 3423 cm^{-1} and the sharp one between 1622÷1627 cm^{-1} are attributed to the hydration water, while the bands located between 719÷725 cm^{-1} and 633÷643 cm^{-1} can be ascribed to Cr-O stretching vibrations [9] (LIB, LIB_V, LIIB_V, LIIA and LIIB). Moreover, the absorption bands located between 1280÷1286 cm^{-1} can be ascribed to the chemisorption process of CO_2 onto Cr_2O_3 surface and the appearance of the so-called negatively charged CO_2 chemisorbates species, i.e., $CO_2^{\delta-}$, while the ones centered between 2355÷2358 cm^{-1} and 2374 cm^{-1} are related to the CO_2 adsorption onto Cr_2O_3 surface [55].

The characteristic absorption bands of $BaSO_4$ include anti-symmetric OH stretching mode of $BaSO_4$ (3423 cm^{-1}), symmetric OH stretching mode, between 2918÷2922 cm^{-1}, symmetric stretching (1622÷1626 cm^{-1}, 984÷985 cm^{-1}), asymmetric stretching (1173÷1179 cm^{-1}) and asymmetric bending vibrations of SO_4^{2-} (633÷637 cm^{-1}, 611 cm^{-1}) [32] (LIB and LIB_V).

The presence of CdS pigment may be indicated only by the absorption bands situated between 719÷724 and 662÷667 cm^{-1} ascribed to the Cd-S stretching vibrations [40] (LIIB).

The main absorption bands of a cobalt-doped zinc oxide structure (CoO·nZnO) can be found between 3393÷3394 and 1081÷1088 cm^{-1} (stretching vibration of H_2O in a Cu-Zn-O lattice), 2355÷2358 cm^{-1} (CO_2 adsorption), 1692÷1697 cm^{-1} (H-OH bending), 747÷750 cm^{-1} (microstructural changes), and between 610÷618 cm^{-1} (stretching of Zn-Cu-O, tetrahedral coordination) [43] (LIIA). A cobalt-doped zinc oxide structure may correspond to either cobalt green or Rinnemann's green pigment.

Ultramarine is the synthetic correspondent of lazurite and contains a similar aluminosilicate framework with Si-O-Si, Al-O-Al and Si-O-Al linkages, the only difference being related to the disorder of Al and Si sites [27]. The characteristic absorption bands of ultramarine can be seen between 1103÷1105 cm^{-1} (Si-O stretching vibrations), 1003÷1008 cm^{-1} (asymmetric stretching of (Si, Al)-O-Si)), and between 712÷713, 699÷703 and 633÷643 cm^{-1} (deformation vibration of SO_4^{2-} associated with the vibrations of Al-Si bond, i.e., symmetric stretching of (Si, Al)-O-Si)) [39] (LIIB_V).

Wax is a kind of material that was often used as a consolidating paint layer for conservation treatments of artworks, either in the form of paraffin wax or beeswax. Furthermore, small amounts of wax impurities can be found in shellac resin. In the present study, the absence of the absorption bands located at around 2935, 2833, 1470 and 1380 cm^{-1} eliminates the possibility of paraffin wax usage [48]. The absorption spectra of beeswax are characterized by the appearance of strong and narrow bands between 3344÷3350 cm^{-1}, 2918÷2921 cm^{-1} and 2850÷2853 cm^{-1}, respectively, due to the stretching vibrations of hydroxyl groups, asymmetric and symmetric stretching vibrations of CH_2 group and CH_3 groups, respectively. Other characteristic absorption bands of beeswax can be observed at 1735 cm^{-1} (C=O stretching), 1712÷1714 cm^{-1} (CO stretching of carboxylic groups), 1173÷1179 cm^{-1} (C-O-C stretching of ester groups) and between 945÷953 cm^{-1} (bending of C–H units), respectively. The distinguishing characteristic of beeswax is the occurrence of two doublets between 1454÷1460 cm^{-1} (CH planar deformation, medium intensity) and 719÷724 cm^{-1} ($\delta(CH_2)_n$, non-planar skeletal deformation, strong intensity) from long n-alkanes, long-chain fatty acids and esters present in beeswax, respectively, this specific feature being related to its semi-crystalline nature. The widening of the absorption bands corresponding to CH groups and the appearance of the hydroxyl absorption band as a rather shoulder of the bands located at around 2900 cm^{-1} may suggest the use of beeswax in a mixture with a resin. The use of pigments in combination with a binder containing both beeswax and oil or application of beeswax over the varnish as a stabilizer for both pigments and bindings was a common practice of the impressionist painters [57].

Although the main C=O stretching band correlated with the presence of common resins like mastic, dammar or sandarac can be found in the 1678÷1705 cm^{-1} region, this band is shifting toward higher wavenumbers (up to 1714 cm^{-1}) due to the ageing process, which can be furthermore connected with the use of shellac as a resin. The other aged shellac absorption bands can be observed between 3393÷3394 cm^{-1} (OH stretching vibrations of carboxylic and hydroxylic groups), 2918÷2922 cm^{-1} (CH_3 stretching), 2850÷2853 cm^{-1} (CH_2 stretching), 1730÷1736 cm^{-1} (C=O stretching), 1643÷1654 cm^{-1} (C=C stretching deriving from jalaric and shellolic acids), 1454÷1460 cm^{-1} (CO stretching, OH deformation of primary/secondary alcohol), 1406÷1414 (OH bending), 1370÷1373 cm^{-1} (CH_3 bending), 1241÷1234 cm^{-1} (COO stretching, CC stretching, CH bending), 1156÷1165 cm^{-1} (COO stretching, CH bending), 1111÷1115 cm^{-1} (CH bending), 1045 cm^{-1} (CO stretching, CH bending), 945÷956 cm^{-1} and between 930÷931 cm^{-1} (CH and OH out-of-plane bending), respectively [46,47].

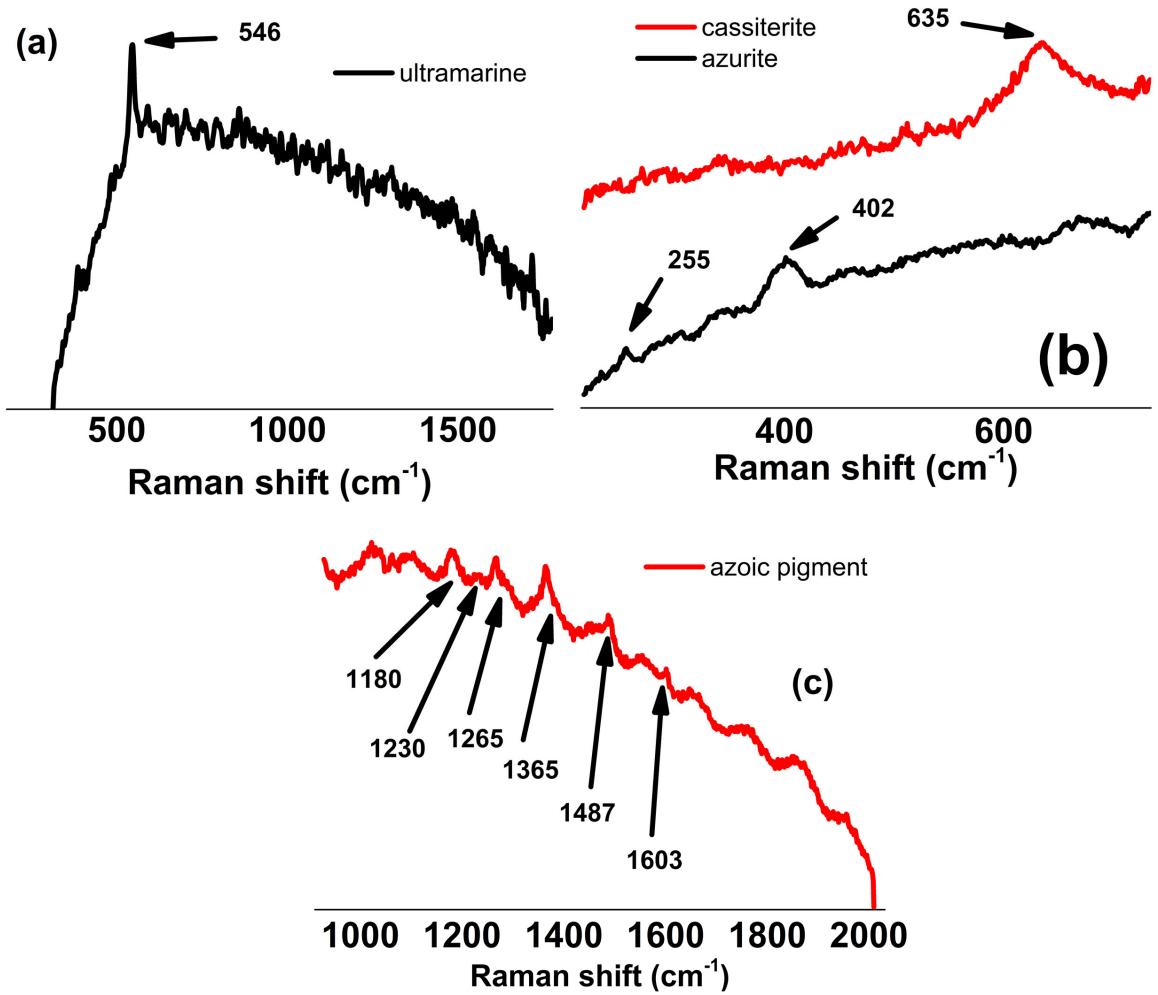


Figure S14. Possible identification of other pigments a) ultramarin by μ-Raman on the paintings themselves, b) azurite and cassiterite by Raman on sample LIIA, c) azoic pigment PR57:1 by Raman on sample LIIA

References

[1] Sano, N.; Cumpson, P.J.; Cwiertnia, E.; Perry, J.J.; Singer, B.W. Multivariate analysis studies of the ageing effect for artist's oil paints containing modern organic pigments. Surf. Interface Anal. 2014, 46, 786-790. https://doi.org/10.1002/sia.5467 (reference [14] from the main manuscript).

[2] Moulder, J.F. *Handbook of X-ray Photoelectron Spectroscopy: A Reference Book of Standard Spectra for Identification and Interpretation of XPS Data*; Perkin-Elmer Corporation, Minnesota, USA, 1992. ISBN 0962702625, 9780962702624 (reference [22] from the main manuscript).

[3] Tingle, T.N.; Borch, R.S.; Hochella, M.F.; Becker, C.H.; Walker, W.J. Characterization of lead on mineral surfaces in soils contaminated by mining and smelting. J. Appl. Surf. Sci. 1993, 72, 301-306. https://doi.org/10.1016/0169-4332(93)90366-J (reference [24] from the main manuscript).

[4] Greczynski, G.; Hultman, L. C 1s peak of adventitious carbon aligns to the vacuum level: dire consequences for material's bonding assignment by photoelectron spectroscopy. ChemPhysChem 2017, 18, 1507-1512. https://doi.org/10.1002/cphc.201700126 (reference [11] from the main manuscript).

[5] NIST X-ray Photoelectron Spectroscopy (XPS) Database (reference [13] from the main manuscript).

[6] Yoshida, T.; Yamaguchi, T.; Iida, Y.; Nakayama, S. XPS study of Pb(II) adsorption on γ-Al2O3 surface at high pH conditions. J. Nucl. Sci. Technol. 2003, 40, 672-678. https://doi.org/10.1080/18811248.2003.9715405 (reference [26] from the main manuscript).

[7] Rasouli, S.; Moeen, S.J. Combustion synthesis of Co-doped zinc oxide nanoparticles using mixture of citric acid–glycine fuels. J. Alloys Compd. 2011, 509, 1915-1919. https://doi.org/10.1016/j.jallcom.2010.10.087 (reference [20] from the main manuscript).

[8] Gandhi, V.; Ganesan, R.; Syedahamed, H.H.A.; Thaiyan, M. Effect of cobalt doping on structural, optical, and magnetic properties of ZnO nanoparticles synthesized by coprecipitation method. J. Phys. Chem. C 2014, 118, 9715-9725. https://doi.org/10.1021/jp411848t (reference [21] from the main manuscript).

[9] Al-Gaashani, R.; Radiman, S.; Daud, A.R., Tabet, Al-Douri, N.Y. XPS and optical studies of different morphologies of ZnO nanostructures prepared by microwave methods. Ceram. Int. 2013, 39, 2283-2292. https://doi.org/10.1016/j.ceramint.2012.08.075 (reference [23] from the main manuscript).

[10] Tingle, T.N.; Borch, R.S.; Hochella, M.F.; Becker, C.H.; Walker, W.J. Characterization of lead on mineral surfaces in soils contaminated by mining and smelting. J. Appl. Surf. Sci. 1993, 72, 301-306. https://doi.org/10.1016/0169-4332(93)90366-J (reference [24] from the main manuscript).

[11] Bartiaux, S.; Lhoest; J.-B.; Genet, M.J.; Bertrand, P.; Rouxhet, P.G. Poly(amino acids) by XPS: analysis of poly(L-serine. Surf. Sci. Spectra 1994, 3, 342–347 (1994). https://doi.org/10.1116/1.1247763 (reference [18] from the main manuscript).

[12] Baltrusaitis, J.; Jayaweera, P.M.; Grassian, V.H. XPS study of nitrogen dioxide adsorption on metal oxide particle surfaces under different environmental conditions. Phys. Chem. Chem. Phys. 2009, 11, 8295-8305. https://doi.org/10.1039/B907584D (reference [19] from the main manuscript).

[13] Baltrusaitis, J.; Usher, C.R.; Grassian, V.H. Reactions of sulfur dioxide on calcium carbonate single crystal and particle surfaces at the adsorbed water carbonate interface. *Phys. Chem. Chem. Phys.* **2007**, *9*, 3011-3024. https://doi.org/10.1039/B617697F (reference [25] from the main manuscript).

[14] Smart, R.S.C.; Skinner, W.M.; Gerson, A.R. XPS of sulphide mineral surfaces: metal-deficient, polysulphides, defects and elemental sulphur. Surf. Interface Anal. 1999, 28, 101-105. https://doi.org/10.1002/(SICI)1096-9918(199908)28:1<101::AID-SIA627>3.0.CO;2-0 (reference [28] from the main manuscript).

[15] Furuyama, M.; Kishi, K.; Ikeda, S. The adsorption of SO2 on iron surfaces studied by x-ray photoelectron spectroscopy. J. Electron. Spectros. Relat. Phenomena 1978, 13, 59-67. https://doi.org/10.1016/0368-2048(78)85007-5 (reference [29] from the main manuscript).

[16] Du, N.; Zhang, H.; Chen, B.; Ma, X.; Liu, Z.; Wu, J.; Yang, D. Porous indium oxide nanotubes: layer-by-layer assembly on carbon-nanotube templates and application for room-temperature NH3 gas sensors. Adv. Mater. 2007, 19, 1641-1645. https://doi.org/10.1002/adma.200602128 (reference [12 from the main manuscript).
[17] Ciomartan, D.A.; Clark, R.J.H.; McDonald, L.J.; Odlyha, M. Studies on the thermal decomposition of basic lead(II) carbonate by Fourier-transform Raman spectroscopy, X-ray diffraction and thermal analysis. J. Chem. Soc. Dalton Trans. 1996, 18, 3639-3645. https://doi.org/10.1039/DT9960003639 (reference [34] from the main manuscript).
[18] White, S.N. Laser Raman spectroscopy as a technique for identification of seafloor hydrothermal and cold seep minerals. Chem. Geol. 2009, 259, 240-252. https://doi.org/10.1016/j.chemgeo.2008.11.008 (reference [29] from the main manuscript).
[19] Cuscó, R.; Alarcón-Lladó, E.; Ibáñez, J.A.L.; Jiménez, J.; Wang, B.; Callahan, M.J. Temperature dependence of Raman scattering in ZnO. Phys. Rev. B 2007, 75, 165202-1-165202-11. doi:10.1103/physrevb.75.165202 (reference [28] from the main manuscript).
[20] Scheuermann, W.; Ritter, G.J.; Schutte, C.J.H. The vibrational spectra of strontium chromate ($SrCrO_4$) and lead chromate ($PbCrO_4$). *Z. Naturforsch*. **1970**, *25*, 1856-1862. https://doi.org/10.1515/zna-1970-1212 (reference [33] from the main manuscript).
[21] Frost, R.L.; Martens, W.N.; Kloprogge, J.T. *N.* Raman spectroscopic study of cinnabar (HgS), realgar (As_4S_4), and orpiment (As_2S_3) at 298 and 77K. *Jb. Miner. Mh.* **2002**, *10*, 469-480. DOI: 10.1127/0028-3649/2002/2002-0469 (reference [30] from the main manuscript).
[22] Legan, L.; Retko, K.; Ropret, P. Vibrational spectroscopic study on degradation of alizarin carmine. *Microchem. J.* **2016**, *127*, 36-45. https://doi.org/10.1016/j.microc.2016.02.002 (reference [32] from the main manuscript).
[23] Vandenabeele, P.; Wehling, B.; Moens, L.; Edwards, H.; De Reu M.; Van Hooydonk, G. Analysis with micro-Raman spectroscopy of natural organic binding media and varnishes used in art. *Anal. Chim. Acta* **2000**, *407*, 261-274. https://doi.org/10.1016/S0003-2670(99)00827-2 (reference [36] from the main manuscript).
[24] Osticioli, I.; Mendes, N.F.C.; Nevin, A.; Gil, F.P.S.C.; Becucci, M.; Castellucci, E. Analysis of natural and artificial ultramarine blue pigments using laser induced breakdown and pulsed Raman spectroscopy, statistical analysis and light microscopy. *Spectrochim. Acta Part A Mol. Biomol. Spectrosc*. **2009**, *73*, 525–531. doi: 10.1016/j.saa.2008.11.028 (reference [37] from the main manuscript).
[25] Donaldson, J.D.; Donoghue, M.T.; Ross, S.D. The vibrational spectra of tetragonal and orthorhombic PbO. *Spectrochim. Acta* **1974**, *30A*, 1967-1975. https://doi.org/10.1016/0584-8539(74)80044-9 (reference [38] from the main manuscript).
[26] Marshall, C.P.; Dufresne, W.J.B.; Rufledt, C.J. Polarized Raman spectra of hematite and assignment of external modes. *J. Raman Spectrosc*. **2020**, *51*, 1522-1529. DOI:10.1002/jrs.5824 (reference [40] from the main manuscript).
[27] Casadio, F.; Bezúr, A.; Fiedler, I..; Muir, K.; Trad, T.; Maccagnola, S. Pablo Picasso to Jasper Johns: a Raman study of cobalt-based synthetic inorganic pigments. *J. Raman Spectrosc*. **2012**, *43*, 1761-1771. https://doi.org/10.1002/jrs.4081 (reference [41] from the main manuscript).
[28] Ferrari, A.C.; Robertson, J. Interpretation of Raman spectra of disordered and amorphous carbon. *Phys. Rev. B* **2000**, *61*, 14095-14107. https://doi.org/10.1103/PhysRevB.61.14095 (reference [42] from the main manuscript).
[29] Taudul, B.; Tielens, F.; Calatayud, M. On the origin of Raman activity in anatase TiO_2 (nano) materials: an *ab initio* investigation of surface and size effects. *Nanomaterials* **2023**, *13*, 1856. https://doi.org/10.3390/nano13121856 (reference [43] from the main manuscript).
[30] P.S.R. Prasad, K. Shiva Prasad, V. Krishna Chaitanya, E.V.S.S.K. Babu, B. Sreedhar, S. Ramana Murthy, In situ FTIR study on the dehydration of natural goethite, Journal of Asian Earth Sciences 27 (2006) 503–511. 10.1016/j.jseaes.2005.05.005.

[31] Lane, M.D. Mid-infrared emission spectroscopy of sulfate and sulfate-bearing minerals. *Am. Min.* **2007**, *92*, 1–18. doi:10.2138/am.2007.2170 (reference [53] from the main manuscript).
[32] B. Prameena, G. Anbalagan, V. Sangeetha, S. Gunasekaran, G.R. Ramkumaar, Behaviour of Indian natural Baryte mineral, International Journal of ChemTech Research, Vol. 5, No. 1, pp 220-231, 2013.
[33] Monico, L.; Rosi, F.; Miliani, C.; Daveri, A.; Brunetti, B.G. Non-invasive identification of metal-oxalate complexes on polychrome artwork surfaces by reflection mid-infrared spectroscopy. Spectrochim. Acta A Mol. Biomol. Spectrosc. 2013, 116, 270-280. https://doi.org/10.1016/j.saa.2013.06.084 (reference [59] from the main manuscript).
[34] https://spectra.chem.ut.ee/paint/binders/rabbitskin-glue/
[35] Riaz, T.; Zeeshan, R.; Zarif, F.; Ilyas, K.; Muhammad, N.; Safi, S.Z.; Rahim, A.; Rizvi, S.A.A.; Rehman, I.U. FTIR analysis of natural and synthetic collagen. Appl. Spectrosc. Rev. 2018, 53, 703–746. doi:10.1080/05704928.2018.1426595.
[36] Pellegrini, D.; Duce, C.; Bonaduce, I.; Biagi, S.; Ghezzi, L.; Colombini, M.P.; Tinè, M.R.; Bramanti, E. Fourier transform infrared spectroscopic study of rabbit glue/inorganic pigments mixtures in fresh and aged reference paint reconstructions. Microchem. J. 2016, 124, 31-35. https://doi.org/10.1016/j.microc.2015.07.018.
[37] Corbeil, M.C.; Charland, J.P.; Moffatt, E.A. The characterization of cobalt violet pigments. Stud. Conserv. 2002, 47, 237-249. doi:10.2307/1506784 (reference [49] from the main article).
[38] Subba Rao, G.V.; Rao, C.N.R.; Ferraro, J.R. Infrared and electronic spectra of rare earth perovskites: ortho-chromites, -manganites and -ferrites. Appl. Spectrosc. 1970, 24, 436-445. https://opg.optica.org/as/abstract.cfm?URI=as-24-4-436.
[39] Ostrooumov, M.; Fritsch, E.; Faulques, E.; Chauvet, O. Spectrometric study of lazurite from the Pamirs, Tajikistan. Can. Mineral. 2002, 40, 885-893.
[40] Muniyappan, S.; Arivunithi, U.M.; Solaiyammal, T.; Sudhakar, K.; Kumar, R.R.; Murugakoothan, P. Synthesis, structural, optical, morphological and elemental characterization of CTAB capped CdS quantum dots by facile chemical precipitation technique. In Recent trends in materials science and applications: nanomaterials, crystal growth, thin films, quantum dots & spectroscopy (Proceedings ICRTMSA 2016); Editor Ebenezar, J.; Spring: Cham, Switzerland, 2017, 341–348. DOI 10.1007/978-3-319-44890-9.
[41] Brooker, M.H.; Sunder, S.; Taylor, P.; Lopata, V.J. Infrared and Raman spectra and X-ray diffraction studies of solid lead(II) carbonates. Can. J. Chem. 1983, 61, 494-502. https://doi.org/10.1139/v83-087 (reference [45] from the main manuscript).
[42] Udvardi, B.; Kovács, I.J.; Kónya, P.; Földvári, M.; Füri, J.; Budai, F.; Falus, G.; Fancsik, T.; Szabó, C.; Szalai, Z.; Mihály, J. Application of attenuated total reflectance Fourier transform infrared spectroscopy in the mineralogical study of a landslide area, Hungary. Sediment. Geol. 2014, 1-14. https://doi.org/10.1016/j.sedgeo.2014.08.005 (reference [47] from the main manuscript).
[43] Ashokkumar, M.; Muthukumaran, S. Microstructure, optical and FTIR studies of Ni, Cu co-doped ZnO nanoparticles by co-precipitation method. Opt. Mater. 2014, 37, 671-678. https://doi.org/10.1016/j.optmat.2014.08.012.
[44] Ferreira, G.R.; Garcia, H.C.; Couri, M.R.C.; Dos Santos, H.F.; de Oliveira, L.F.C. On the azo/hydrazo equilibrium in Sudan I azo dye derivatives. J. Phys. Chem. A 2013, 117, 642-649. https://doi.org/10.1021/jp310229h (reference [48] from the main manuscript).
[45] Bharat, L.K.; Reddy, L.S.; Yu, J.S. Sol–gel synthesis, characterization and photocatalytic properties of SrCrO4 particles. Mater. Lett. 2015, 144, 85-89. https://doi.org/10.1016/j.matlet.2015.01.021 (reference [46] from the main manuscript).

[46] http://lisa.chem.ut.ee/IR_spectra/coating_materials/shellac/.
[47] Ciofini, D. Removal of Varnish and Overpaint Layers from Easel Paintings using Pulsed Nd:YAG Lasers. PhD thesis, Università degli Studi di Firenze, Firenze, 2014.
[48] Shearer, G.L. An Evaluation of Fourier Transform Spectroscopy for the Characterization of Organic Compounds in Art and Archaeology. PhD thesis, University College, London, 1989.
[49] Morsch, S.; Van Driel, B.A.; van den Berg, K.J.; Dik, J. Investigating the photocatalytic degradation of oil paint using ATR-IR and AFM-IR. ACS Appl. Mater. Interfaces. 2017, 9, 10169–10179. doi:10.1021/acsami.7b00638 (reference [55] from the main manuscript).
[50] Izzo, F. C., Kratter, M., Nevin, A., & Zendri, E. (2021). A Critical Review on the Analysis of Metal Soaps in Oil Paintings. ChemistryOpen, 10(9), 904–921. doi:10.1002/open.202100166.
[51] Otero, V.; Sanches, D.; Montagner, C.; Vilarigues, M.; Carlyle, L.; Lopes. J.A.; Melo, M.J. Characterisation of metal carboxylates by Raman and infrared spectroscopy in works of art. *J. Raman Spectrosc.*, **2014**, *45*, 1197-1206. https://doi.org/10.1002/jrs.4520 (reference [56] from the main manuscript).
[52] Silva, Izabela & Sánchez, Benigno & Canela, Maria. (2023). Lead Carboxylates and Chromatic Parameter Changes in Oil-Based Paintings Exposed to Volatile Organic Compounds. Journal of the Brazilian Chemical Society. 34. 10.21577/0103-5053.20230069.
[53] Alfred A. Christy, Per K. Egeberg, Quantitative determination of saturated and unsaturated fatty acids in edible oils by infrared spectroscopy and chemometrics, Chemometrics and Intelligent Laboratory Systems, Volume 82, Issues 1–2, 2006, Pages 130-136, ISSN 0169-7439, https://doi.org/10.1016/j.chemolab.2005.06.019.
[54] Hermans, J. J., Keune, K., van Loon, A., & Iedema, P. D. (2015). An infrared spectroscopic study of the nature of zinc carboxylates in oil paintings. Journal of Analytical Atomic Spectrometry, 30(7), 1600–1608. doi:10.1039/c5ja00120j.
[55] Seiferth, O.; Wolter, K.; Dillmann, B.; Klivenyi, G.; Freund, H.-J.; Scarano, D.; Zecchina, A. IR investigations of CO_2 adsorption on chromia surfaces: Cr_2O_3 (0001)/Cr(110) versus polycrystalline α-Cr_2O_3. Surf. Sci. 1999, 421, 176-190. https://doi.org/10.1016/S0039-6028(98)00857-7.
[56] Klinowski, J.; Carr, S.W.; Tarling, S.E.; Barnes, P. Magic-angle-spinning NMR shows the aluminosilicate framework of ultramarine to be disordered. *Nature* **1987**, *330*, 56-58. DOI 10.1038/330056a0.
[57] M. Regert, S. Colinart, L. Degrand and O. Decavallas, Chemical Alteration and Use of Beeswax Through Time: Accelerated Ageing Tests and Analysis of Archaeological Samples from Various Environmental Contexts, Archaeometry, 2001, 43, 549-569. **https://doi.org/10.1111/1475-4754.00036.**